Momentum-resolved electronic structure at a buried interface from soft X-ray standing-wave angle-resolved photoemission

Momentum-resolved electronic structure at a buried interface from soft X-ray standing-wave angle-resolved photoemission

A. X. Gray[1,2,3], J. Minár[4], L. Plucinski[5], M. Huijben[6], A. Bostwick[7], E. Rotenberg[7], S.-H. Yang[8], J. Braun[4], A. Winkelmann[9], G. Conti[1,2], D. Eiteneer[1,2], A. Rattanachata[1,2], A. A. Greer[1,2], J. Ciston[10], C. Ophus[10], G. Rijnders[6], D. H. A. Blank[6], D. Doennig[11], R. Pentcheva[11], J. B. Kortright[2], C. M. Schneider[5], H. Ebert[4] and C. S. Fadley[1,2]

[1] *Department of Physics, University of California Davis - Davis, CA 95616, USA*
[2] *Materials Sciences Division, Lawrence Berkeley National Laboratory - Berkeley, CA 94720, USA*
[3] *Stanford Institute for Materials and Energy Science, Stanford University and SLAC National Accelerator Laboratory 2575 Sand Hill Road, Menlo Park, CA, 94029, USA*
[4] *Department of Chemistry, Physical Chemistry Institute, Ludwig-Maximilians University-Munich - München, Germany*
[5] *Peter-Grünberg-Institut PGI-6, Forschungszentrum Jülich GmbH - 52425 Jülich, Germany*
[6] *Faculty of Science and Technology, MESA+ Institute for Nanotechnology, University of Twente - Enschede, The Netherlands*
[7] *Advanced Light Source, Lawrence Berkeley National Laboratory - Berkeley, CA 94720, USA*
[8] *IBM Almaden Research Center - San Jose, CA 95120, USA*
[9] *Max-Planck-Institut für Mikrostrukturphysik - Weinberg 2, D-06120 Halle (Saale), Germany*
[10] *National Center for Electron Microscopy, Lawrence Berkeley National Laboratory - Berkeley, CA 94720, USA*
[11] *Department of Earth and Environmental Sciences and Center of Nanoscience (CENS), Ludwig-Maximilians University-Munich - München, Germany*

Abstract – Angle-resolved photoemission spectroscopy (ARPES) is a powerful technique for the study of electronic structure, but it lacks a direct ability to study buried interfaces between two materials. We address this limitation by combining ARPES with soft X-ray standing-wave (SW) excitation (SWARPES), in which the SW profile is scanned through the depth of the sample. We have studied the buried interface in a prototypical magnetic tunnel junction $La_{0.7}Sr_{0.3}MnO_3/SrTiO_3$. Depth- and momentum-resolved maps of Mn $3d$ e_g and t_{2g} states from the central, bulk-like and interface-like regions of $La_{0.7}Sr_{0.3}MnO_3$ exhibit distinctly different behavior consistent with a change in the Mn bonding at the interface. We compare the experimental results to state-of-the-art density-functional and one-step photoemission theory, with encouraging agreement that suggests wide future applications of this technique.

Introduction. – Angle-resolved photoemission (ARPES) is the technique of choice for probing the electronic structure of solids and surfaces, yielding as direct output a map of photoelectron intensities as a function of the electron kinetic energy E_{kin} and electron momentum $\vec{p} = \hbar\vec{k}$, and it has been applied to virtually every type of crystalline, or even quasicrystalline material [1,2]. A typical experimental setup involving a hemispherical electrostatic analyzer is shown in fig. 1(a). For excitation

with a photon energy $h\nu$, three-dimensional datasets of kinetic energy $E_{kin}(\vec{k})$ or binding energy relative to the Fermi level $E_b^F(\vec{k}) \approx h\nu - E_{kin}(\vec{k})$ as a function of the k_x and k_y components are obtained by measuring detector images of E_{kin} vs. the take-off angle θ_{TOA} and scanning also the orthogonal angle β_{TOA} by rotating the sample. Each point in this volume can in turn be mapped into the reduced Brillouin zone (BZ) via direct transitions (DTs) that in their simplest form obey the conservation law
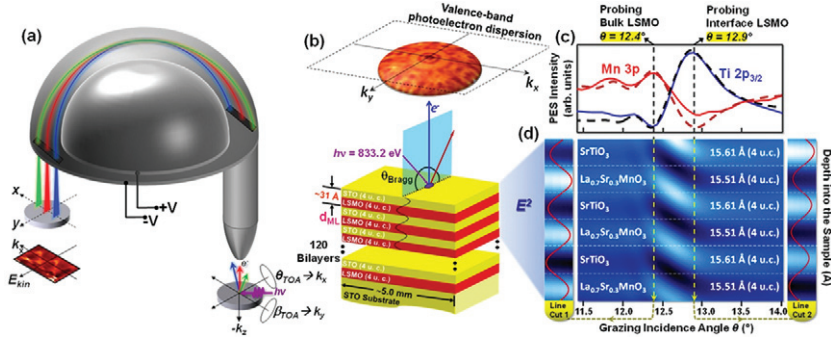
Fig. 1: (Color online) Experimental setup and basic principles of standing-wave (SW) ARPES (SWARPES). (a) Schematic diagram of the ARPES experiment illustrating the angular degrees of freedom for the sample manipulation (θ_{TOA} and β_{TOA}), the hemispherical electrostatic photoelectron analyzer, the position-sensitive multichannel plate (MCP) detector with two orthogonal axes $x = k_x$ and $y = E_{kin}$, and the final CCD screen with the resulting E_{kin} *vs.* k_x dispersion. The angle between photon incidence and the spectrometer lens axis was $60°$, with both directions lying in the x-z plane. (b) Schematic diagram of the investigated multilayer structure consisting of 120 bilayers of STO and LSMO grown epitaxially on a single-crystal STO substrate, with each bilayer consisting of 4 units cells (15.61 Å) of STO and 4 unit cells (15.51 Å) of LSMO. A photon energy of 833.2 eV corresponding to the maximum reflectivity at the La $3d_{5/2}$ absorption edge was used for the photoemission experiments [17]. An example of the $E_{kin}(\vec{k})$ distribution for a fixed value of the binding energy E_B is shown above the sample. (c) SW-excited photoemission intensity rocking curves (RCs) for Ti $2p_{3/2}$ and Mn $3p$ core-levels (solid curves), as well as the X-ray optical simulations fitted to them (dashed curves), and previously yielding the chemical depth profile of the sample [17]. (d) Simulated intensity of the X-ray SW electric field (E^2) inside the sample as a function of the depth and grazing incidence angle. The line-cuts indicate that, for incidence angles $<12.4°$, the SW field highlights the bulk or center of the LSMO layer, but for angles $>12.9°$ the interface regions of the LSMO layer are emphasized.

$\vec{k} = \vec{k}_i + \vec{g}_{hk\ell} + \vec{k}_{h\nu}$, where $\vec{k}_i$ is in the reduced BZ, $\vec{g}_{hk\ell}$ is a bulk reciprocal lattice vector, and $\vec{k}_{h\nu}$ is the photon wave vector, which must be considered for energies in the soft and hard X-ray regimes above about 0.5 keV due to non-dipole effects [3,4].

However, a significant disadvantage of the conventional ARPES technique is its extreme surface sensitivity, due to the very low inelastic mean-free paths (IMFPs) of the electrons photoemitted using radiation in the range $25\,\text{eV} < h\nu < 150\,\text{eV}$ [5]. As a quantitative example, the IMFP, which is in turn the average depth in normal emission, for the complex oxides $SrTiO_3$ or $La_{0.7}Sr_{0.3}MnO_3$ of interest here can be estimated to be about 1.9 Å at $h\nu = 25\,\text{eV}$, and 5.9 Å at $h\nu = 150\,\text{eV}$ [5,6], or only a couple of atomic layers below the surface. A recent ARPES study of $La_{0.7}Sr_{0.3}MnO_3$ illustrates this surface sensitivity [7]. This has led in recent years to more bulk-sensitive ARPES measurements at higher photon energies and thus larger IMFPs in the 10–100 Å range that are by now being carried out in the soft X-ray regime of 500–1200 eV for various materials [3,4,8–11], as well as in the hard X-ray regime from 3.2 to 5.9 keV [12,13].

Yet, even at these higher photon energies, the photoemission signal originating closer to the surface will be stronger than the signal originating from below according to $I(z) = I_0 \exp[-z/\Lambda \sin \theta_{TOA}]$, where z is the depth, Λ is the IMFP, or more correctly the effective attenuation length (EAL) that includes elastic scattering effects as well [5] and θ_{TOA} is the electron take-off angle relative to the surface (cf. fig. 1(a)) [5,6]. Controllable depth selectivity can however be accomplished by setting up an X-ray

standing-wave (SW) field in the sample by growing it as, or on, a synthetic periodic multilayer mirror substrate, which in first-order Bragg reflection acts as a strong SW generator [14,15]. The maxima of the SW can be moved in the z-direction perpendicular to the sample surface by scanning the incidence angle θ_{inc} through the Bragg condition, thus generating a well-known rocking curve (RC) of intensity [14–16]. Angle-integrated SW-excited X-ray photoemission (SW-XPS) from core-levels and valence bands has been applied previously in studies of various systems, in particular layers and interfaces of relevance to giant magnetoresistance (GMR) and tunnel magnetoresistance (TMR) [16], including the insulator/half-metallic ferromagnet system $SrTiO_3/La_{0.7}Sr_{0.3}MnO_3$ (STO/LSMO) that is the topic of this study [17], but $\vec{k}$-resolved ARPES has not previously been attempted. These prior SW-XPS studies were carried out at room temperature, such that phonon-induced non-direct transitions (NDTs) led to an averaging over the BZ, and resultant valence spectra that closely resemble matrix-element weighted densities of states (MEW-DOS) [3,4]. It is possible to estimate the fraction of DTs from a photoemission Debye-Waller factor of the form $W(T) = \exp[-\frac{1}{3} g_{hk\ell}^2 \langle U^2(T) \rangle]$, where $U^2(T)$ is the three-dimensional mean-squared vibrational displacement [3,4], and we consider this aspect further below and in our Supplementary Information (SI) [18].

In this letter, we add depth selectivity to ARPES by combining more bulk-sensitive soft X-ray excitation at ca. 800 eV corresponding to IMFPs of about 19 Å with the SW approach (SWARPES) to provide a unique depth- and $\vec{k}$-resolved probe of buried layer and interface electronic

structure. Interface electronic structure is known to be crucial to the properties of various nanoscale multilayer systems, as for example, in the magnetic tunnel junction (MTJ) Fe/MgO, for which the Δ_1 band of Fe is thought to be the predominant carrier of spin-polarized tunneling current [19,20], and the interface between STO and LAO in the system $LaAlO_3/SrTiO_3$, for which the interface provides a 2D electron gas that has been shown to be both ferromagnetic and superconducting [21]. Yet there are up to now no techniques for directly studying the interface electronic structure in a $\vec{k}$-resolved manner. We illustrate the capability of SWARPES to do this for a prototypical oxide MTJ, $La_{0.7}Sr_{0.3}MnO_3/SrTiO_3$ (LSMO/STO) by comparing experiment to theory of several types, including, in particular, state-of-the-art one-step photoemission calculations.

The much-studied LSMO/STO system is a promising candidate for a MTJ [22–24], wherein the half-metallic nature of ferromagnetic LSMO is responsible for producing a 100% spin-polarized tunneling current across the STO insulating barrier [25,26]. Up to now, however, the theoretically predicted TMR effect of 100% [27] has not been realized, with the highest TMR values reported so far being on the order of 80% [28–30]. The most widely accepted explanation for this reduced performance is highly localized interface effects in the LSMO layer near the interface with STO [31]. In a prior angle-integrated SW-XPS study of LSMO/STO [17], we have investigated the chemical and electronic structure profiles of the LSMO/STO interface via *core-level* soft and hard X-ray SW-excited photoemission, X-ray absorption and X-ray reflectivity, in conjunction with X-ray optical [32] and core-hole multiplet theoretical modeling [33,34] Analysis of the core-level SW modulations revealed the presence of an interdiffusion region of 4–5 Å in thickness (a little over 1 unit cell) between the STO and LSMO layers, a change in the soft X-ray optical coefficients of LSMO near the interface, and a shift in the position of the Mn $3p$ peak near the interface that is consistent with a crystal-field distortion effect. What is still needed however is depth- and $\vec{k}$-resolved information concerning the valence electronic states. We show here that SWARPES can provide this.

The LSMO/STO multilayer sample consisted of 120 bilayers, each consisting of 4 unit cells of LSMO (~15.51 Å) and 4 unit cells of STO (~15.61 Å), with STO terminating the structure, as shown schematically in fig. 1(b), and was fabricated using the pulsed laser deposition (PLD) technique (see details in the SI [18]). The transport and magnetic properties of the LSMO/STO superlattice are consistent with previous reports [35], as shown in our SI [18].

The SWARPES measurements were carried out at the Electronic Structure Factory (ESF) endstation at Beamline 7.0.1 of the Advanced Light Source (Lawrence Berkeley National Laboratory) using a Scienta R4000 spectrometer. The measurements were performed at a temperature of 20 K and with an overall energy resolution of ~300 meV, with some reference data taken at 300 K. In order to maximize reflectivity and thus also the contrast of the SW, and therefore to better define the depth-resolved photoemission within the sample, the excitation energy was set to 833.2 eV, which is just below the La $3d_{5/2}$ absorption edge, as discussed elsewhere [17].

In order to verify the presence of the SW in the superlattice, and to most quantitatively model the intensity profile of it within the sample, we first performed core-level SW-XPS measurements. Strong SW RC intensity modulations near the Bragg condition for the superlattice were observed for Ti $2p_{3/2}$ and Mn $3p$ core-levels (solid curves in fig. 1(c); these are fully consistent with our prior study of a similar LSMO/STO sample [17]. These RCs were fitted using a specially written theoretical code [32] in order to confirm the chemical profile of the structure with angstrom level accuracy, and the best-fit theoretical curves are shown as dashed curves in fig. 1(c). The conclusions of this SW-XPS analysis were also verified by sub-angstrom scanning transmission electron microscopy (STEM) and electron energy loss spectroscopy (EELS), as discussed in our SI [18]. The same X-ray optical model and sample configuration were then used to simulate the electric-field intensity (E^2) profile of the SW inside the superlattice as a function of depth and incidence angle. The results of these simulations in fig. 1(d) reveal that the SW maxima will highlight the center ("bulk") region of the buried LSMO layer at an incidence angle of 12.4° (a maximum of Mn $3p$ intensity), as shown in the left line-cut. Increasing the incidence angle past the Bragg condition, we shift the SW downwards by about half-a-period, highlighting the interfacial region of the LSMO layer at angles above 12.9° (a maximum of Ti $2p$ intensity), as shown in the right line-cut.

Three-dimensional SWARPES measurements were thus performed at these two incidence angles, as well as others, finally yielding $E_B^F(k_x, k_y(k_z))$, with k_z implicitly known but not directly measured. To validate our final conclusions, we have also measured SWARPES at an additional five angles to the left (11.82°, 12.10°) and right (13.35°, 13.90°) of the RC, as well as in the middle of it (12.15°); some of these results at other angles are presented in our SI [18]. As noted in prior higher-energy ARPES studies [11–13], it is useful to correct such data for the effects of phonon-induced MEW-DOS–like background intensity, as well as X-ray photoelectron diffraction (XPD) effects, which in our SWARPES data can be estimated from the relevant Debye-Waller factors to represent ca. 25% of the intensity. Correction for DOS and XPD effects can to first order be done by dividing the data successively by the average over angle and the average over energy of each detector image, respectively [36] as demonstrated for experimental data from W and GaAs recently [12,13]. Here we have also taken the XPD correction one step further by measuring the Mn $3p$ core-level, as discussed in detail in our SI [18]: however, none of our final conclusions depends on this additional correction.

In fig. 2, we now show some key SWARPES results for five key binding-energy positions, all corrected in the same two-step way to remove any DOS or XPD effects. Figure 2(a) shows a reference, angle-integrated spectrum spanning the Fermi-referenced binding-energy window from $+1\,\text{eV}$ to $-9\,\text{eV}$, including five major features labeled 1–5; this curve, obtained at room temperature, should roughly represent the MEW-DOS for the sample. The region between the binding energies of $0\,\text{eV}$ and $-3.25\,\text{eV}$ contains the LSMO-derived states, specifically Mn $3d\ e_g$ (feature 1, at ca. $1.0\,\text{eV}$) and Mn $3d\ t_{2g}$ (feature 2, at ca. $2.4\,\text{eV}$), and no STO-derived states due to the bandgap "window" [18,37]. Conversely, the region between $-3.25\,\text{eV}$ and $-7.0\,\text{eV}$ we expect to be dominated by the states originating in the topmost STO layer (labeled 3, 4, and expected to be relatively flat complex bands). The deeper bands from LSMO will also show up in this region, but with attenuated intensity due to the STO layer. However, we finally suggest that feature 5 is predominantly LSMO-derived, and show evidence below and in our SI [18] for this interpretation. Figures 2(b), (c) and (d) now show the corrected low-temperature ARPES intensity maps in (k_x, k_y) summed over $300\,\text{meV}$ intervals centered at binding energies 1–5 for the bulk-LSMO–sensitive incidence angle (b), the interface-sensitive angle (c), and the bulk-minus-interface difference between the two (d). The contrast of the color map in the difference map of fig. 2(d) is enhanced in order to accentuate the smaller differences between the bulk-like and interface-like features. Note the indication of the surface normal and the first Brillouin zone in the image in fig. 2(b). Multiple Brillouin zones are thus represented in these images due to the large k vector of a photoelectron at $833.2\,\text{eV}$ excitation energy $(14.8\,\text{Å}^{-1}$, compared to the BZ dimensions in STO or LSMO of $2\pi/a \approx 1.61\,\text{Å}^{-1})$, and the fact that the combined detector image and β_{TOA} scan span $35°$ in k_x and $40°$ in k_y.

The bulk- and interface-sensitive maps at a given energy are at first sight very similar, although those for different energies clearly differ markedly from one another. The most dispersive features 1, 2, and 5 show the most structure, and the less dispersive STO bands 3 and 4 show much less structure. Feature 5 is striking in showing a remarkably simple square pattern that essentially represents the expected BZ repeat pattern; this simple appearance additionally confirms the validity of our DOS and XPD correction procedures. The bulk-minus-interface maps are finally crucial indicators of changes in the electronic structure at the interface. The biggest changes (up to $\sim 4.5\%$ in intensity) are observed for the LSMO-derived Mn $3d$ e_g and t_{2g} electronic states at energies 1 and 2, suggesting significant changes in the (k_x, k_y) dependence of these states at the LSMO/STO interface, including a general suppression of intensity. The STO-dominated states at the binding energies of 4.0 and $6.2\,\text{eV}$ show less momentum dispersion in general, and thus also exhibit only minor
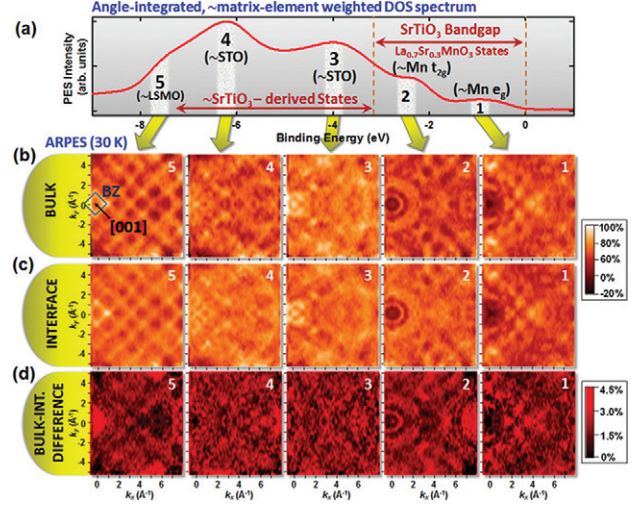

Fig. 2: (Color online) Depth-resolved SWARPES measurements of the LSMO/STO superlattice. (a) An angle-integrated spectrum spanning a binding-energy window of $10\,\text{eV}$ (from $+1\,\text{eV}$ to $-9\,\text{eV}$), and including all the major features of the valence bands, labeled 1–5, with their origins and characters indicated. (b) SWARPES data for these five energies in a bulk-LSMO-sensitive SW measurement geometry. Binding-energy integration windows of $300\,\text{meV}$ (consistent with our total energy resolution) centered around the binding energies of the five features discernible in the angle-integrated valence spectra (as determined by peak-fitting), were used to obtain these plots. Shown are XPD-normalized angle-resolved (k_x, k_y) photoemission intensity maps of the Mn $3d$ e_g (1), Mn $3d$ t_{2g} (2) states, the largely STO-derived states (3 and 4), and the valence band bottom states (5) due largely to LSMO. (c) As (b), but for an LSMO/STO-interface–sensitive measurement geometry of the SW. (d) Bulk-interface difference (k_x, k_y) maps based on (b) and (c), revealing the most significant differences for the LSMO-derived Mn $3d$ e_g and Mn $3d$ t_{2g} states at the interface between STO and LSMO, and as well as the dispersive valence band bottom bands 5 from LSMO. The intensity scales at right indicate the relative amplitudes of the effects.

bulk-interface changes. Finally, the local-density theory shown in our SI [18] indicates that the largely LSMO-derived states 5 at $\sim 7.5\,\text{eV}$ also exhibit a marked change in the (k_x, k_y) dependence near the interface. All of these changes, although subtle, represent a unique experimental insight into the interface electronic structure, and we have verified the validity of these bulk-surface difference effects by making similar difference maps for points on either side of the RC, which are found to show no discernible effects (see our SI [18]).

In comparing our experimental results to theory, we will consider only k-space maps for the LSMO-derived features 1 and 2 representing Mn $3d$ t_{2g} and e_g states, and feature 5 at the bottom of the valence bands that exhibits a very simple dispersion pattern. Figure 3(a) first presents the results of simple free-electron final-state calculations involving direct transitions from LSMO band-structure calculations performed using the Wien2k code at the local density approximation $+$ U (LDA $+$ U) level to allow for
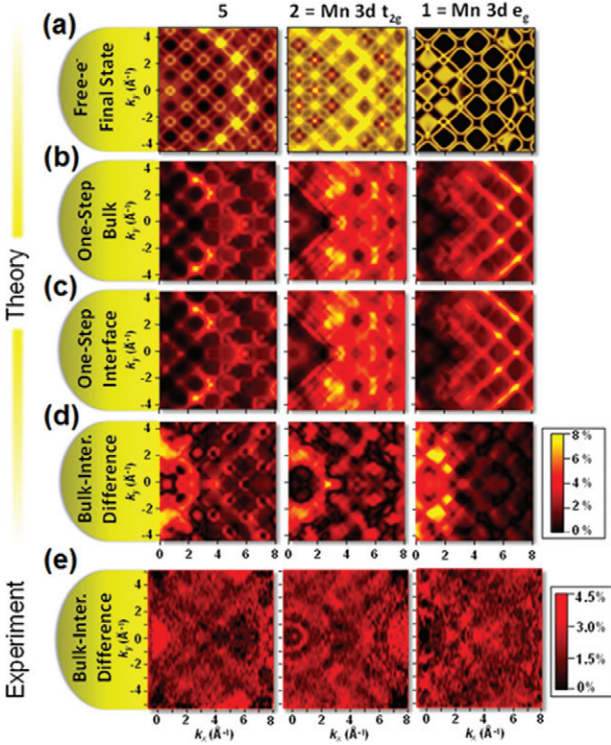
Fig. 3: (Color online) Theoretical calculations for SWARPES from levels Mn $3d$ e_g (1), Mn $3d$ t_{2g} (2) and the bottom of the valence bands (5). (a) Simple free-electron final-state theory with direct transitions from an LDA+U-based band structure (see our SI [18]). Yellow corresponds to spin-up (majority) bands, and red to spin-down (minority). (b), (c), and (d) More accurate one-step photoemission theory summing over both spin polarizations and with the SW intensity profile included, for a bulk-LSMO–sensitive geometry (b), an interface-sensitive geometry (c), and the bulk-minus-interface difference (d), respectively. The amplitudes of the effects are again indicated. (e) represents a direct comparison to experimental panels from fig. 2(d).

correlation effects [38]. Here the LSMO is assumed to be ferromagnetic and the spin of the photoelectrons is distinguished by color (red = majority, yellow = minority); thus the e_g allowed transitions are all majority or red. The agreement between the experiment and theory is very encouraging for all three energies, with the BZ periodicity and positions of some of the major features reproduced well, although of course there is no information in these k-space maps as to relative photoemission intensities, since no allowance is made for matrix elements. Analyzing feature 5 with the LSMO band structure is also found to be valid from LDA calculations for the full multilayer, which predict that the valence band minimum of LSMO is below that of STO (see our SI [18]).

In figs. 3(b)–(d) we present the results of a much more accurate one-step photoemission theory based on a fully relativistic LDA+U layer-KKR (Korringa-Kohn-Rostoker) approach and a time-reversed LEED

(low-energy electron diffraction) final state [39] (further details in our SI [18]), as applied to the actual multilayer structure with the explicitly included surface. These calculations furthermore incorporate a first attempt to include the intensity profile of the X-ray SW by using as an additional input the $|E^2|$ profiles shown in fig. 1(d). The resulting bulk- and interface-sensitive photoemission intensity k-space maps are shown in figs. 3(b), (c). Finally, differences between the bulk and interface electronic structure were calculated and these are plotted in fig. 3(d), and compared to experiment in fig. 3(e). It is important to note that this type of one-step theory calculation represents a much more accurate theoretical counterpart to this particular experiment as compared to the free-electron final-state theory, since in addition to calculating true angular distributions of photoemission intensities due to SW excitation, the influence of the top STO overlayer is also taken into account, albeit in a rigid lattice approximation so that phonon effects are not included. Thus, although the periodicity of the BZs and the positions of the major features are similar to those in fig. 3(a), visible differences are observed between the k-space maps generated using these two theoretical approaches.

Comparing the results of the one-step theory calculations to the experimental k-space maps we observe encouraging similarities. In particular, the sizes of the BZ features, and the general intensity variations across the image, with noticeable depression in intensities in the first BZ (including e_g intensity loss in fig. 2(b), (c)), are well reproduced. Most importantly, the bulk-interface difference maps for the LSMO-derived Mn $3d$ e_g and t_{2g} states show a similar degree of suppression in intensities at the LSMO/STO interface —about 9.5% in theory compared to 4.5% in experiment. Thus, although we cannot yet claim a fully quantitative agreement between experiment and theory, these results demonstrate a significant first step in the interpretation and use of interface-resolved SWARPES data.

In conclusion, by combining soft X-ray ARPES with SW-excited photoelectron spectroscopy, we have devised a unique technique for probing the $\vec{k}$-resolved electronic structure of buried layers and interfaces. By generating an X-ray SW inside a multilayer sample, and then translating it up and down within the sample by varying the incidence angle, we can selectively probe the electronic structure emphasizing the bulk of a layer or its interface, and then directly compare the two. We have applied SWARPES to the investigation of the electronic properties of the buried interface within a magnetic tunnel junction composed of $La_{0.7}Sr_{0.3}MnO_3/SrTiO_3$, and discovered that the bulk-like and interface-like regions of the buried $La_{0.7}Sr_{0.3}MnO_3$ layer exhibit a distinctly different behavior, consistent with a change in the Mn bonding geometry at the $La_{0.7}Sr_{0.3}MnO_3/SrTiO_3$ interface observed previously [17], but now elaborated with $\vec{k}$ resolution. The experimental results are further validated via agreement

with free-electron final-state model calculations and more precise state-of-the-art one-step photoemission theory including matrix-element effects. Future theoretical treatments should involve the inclusion of atomic distortions near the interface, *e.g.* incorporating a crystal-field distortion near the interface that is suggested by our prior angle-integrated SW-XPS study of the same system [17] and more detailed calculations presented in our SI [18], as well as a more accurate inclusion of the interface mixing/roughness that is also seen in the prior SW-XPS study of this system [17], as well as TEM + EELS data from the present sample [18], the SW intensity profile and phonon effects. We thus suggest that the SWARPES method should be of broad use in the future studies of buried layers and interfaces in various types of epitaxial multilayer structures, including those exhibiting spintronic, ferroelectric, multiferroic, and superconducting properties

* * *

REFERENCES

[1] Damascelli A., Hussain Z. and Shen Z.-X., *Rev. Mod. Phys.*, **75** (2003) 473.
[2] Lu D. H. *et al.*, *Annu. Rev. Condens. Matter Phys.*, **3** (2012) 129.
[3] Plucinski L. *et al.*, *Phys. Rev. B*, **78** (2008) 035108.
[4] Papp C. *et al.*, *Phys. Rev. B.*, **84** (2011) 045433.
[5] Powell C. J. *et al.*, *J. Electron Spectrosc. Relat. Phenom.*, **98** (1999) 1.
[6] Tanuma S., Powell C. J. and Penn D. R., *Surf. Interface Anal.*, **43** (2011) 689.
[7] Krempasky J. *et al.*, *J. Electron Spectrosc. Relat. Phenom.*, **181** (2010) 63.
[8] Sekiyama, A. *et al.*, *Nature*, **403** (2000) 396.
[9] Iwasaki T. *et al.*, *Phys. Rev. B*, **65** (2002) 195109.
[10] Claesson T. *et al.*, *Phys. Rev. Lett.*, **93** (2004) 136402.
[11] Fadley C. S., *Synchrotron Radiat. News*, **25** (2012) 26.
[12] Gray A. X. *et al.*, *Nat. Mater.*, **10** (2011) 759.
[13] Gray A. X. *et al.*, *Nat. Mater.*, **11** (2012) 957.
[14] Yang S.-H. *et al.*, *Surf. Sci.*, **461** (2000) L557.
[15] Yang S.-H. *et al.*, *J. Phys.: Condens. Matter*, **14** (2002) L407.
[16] Yang S.-H. *et al.*, *J. Phys.: Condens. Matter*, **18** (2006) L259.
[17] Gray A. X. *et al.*, *Phys. Rev. B*, **82** (2010) 205116.
[18] Supplementary Information available online at `http://www.physics.ucdavis.edu/fadleygroup/SWARPES-SI.pdf`.
[19] Butler W. H., Zhang X.-G., Schulthess T. C. and MacLaren J. M., *Phys. Rev. B*, **63** (2001) 054416.
[20] Heiliger C., Zahn P., Yavorsky B. Y. and Mertig I., *Phys. Rev. B*, **73** (2006) 214441.
[21] Bert J. A., Kalisky B., Bell C., Kim M., Hikita Y., Hwang H. Y. and Moler K. M., *Nat. Phys.*, **7** (2011) 767.
[22] De Teresa J. M. *et al.*, *Phys. Rev. Lett.*, **82** (1999) 4288.
[23] Wolf S. A. *et al.*, *Science*, **294** (2001) 1488.
[24] Tsymbal E. Y., Mryasov O. N. and LeClair P. R., *J. Phys.: Condens. Matter*, **15** (2003) R109.
[25] Ma C., Yang Z. and Picozzi S., *J. Phys.: Condens. Matter*, **18** (2006) 7717.
[26] Chikamatsu A. *et al.*, *Phys. Rev. B*, **73** (2006) 195105.
[27] Park J.-H. *et al.*, *Nature*, **392** (1998) 794.
[28] Yu Lu, Li X. W., Gong G. Q. and Gang Xiao, *Phys. Rev. B*, **54** (1996) R8357.
[29] Sun J. Z. *et al.*, *Appl. Phys. Lett.*, **69** (1996) 3266.
[30] Viret M. *et al.*, *Europhys. Lett.*, **39** (1997) 545.
[31] Izumi M. *et al.*, *Phys. Rev. B*, **64** (2001) 064429.
[32] Yang S.-H. *et al.*, *J. Appl. Phys.*, **113** (2013) 073513.
[33] De Groot F. M. F. and Kotani A., *Core Level Spectroscopy of Solids* (Taylor & Francis, London) 2008.
[34] Stavitski E. and De Groot F. M. F., *CTM4XAS Charge Transfer Multiplet Program* (2010).
[35] Fitting Kourkoutis L., Song J. H., Hwang H. Y. and Muller D. A., *Proc. Natl. Acad. Sci. U.S.A.*, **107** (2010) 11682.
[36] Bostwick A. and Rotenberg E., private communication.
[37] Kumigashira H. *et al.*, *J. Appl. Phys.*, **99** (2006) 08S903.
[38] Blaha P., Schwarz K., Madsen G., Kvasnicka D. and Luitz J., *WIEN2k, An Augmented Plane Wave + Local Orbitals Program for Calculating Crystal Properties* (Technische Universität Wien) 2001, ISBN 3-9501031-1-2.
[39] Braun J., Minár J., Ebert H., Katsnelson M. I. and Lichtenstein A. I., *Phys. Rev. Lett.*, **97** (2006) 227601.